THERMAL BLOOMING OF OPTICAL BEAM IN A HEAT–CONDUCTING AND VISCOUS GAS UNDER GRAVITATIONAL CONVECTION

A.N. Kucherov

N.E. Zhukovskii Central Aerohydrodynamics Institute, Moscow
Received August 22, 1993

Theoretical investigation of thermal blooming of a horizontally propagating optical beam with a self–induced gravitational convection is carried out using numerical simulations. The thermal conductivity and viscosity of a gas are taken into account. The results are compared with the analogous experimental data.

The process of radiation propagation through the resting medium (or at the segments of relative rest, i.e., in the "immobile" zones) within the time interval $t_c = (\rho_0 h_0 a/q_0 g)^{1/3}$ causes the natural gravitational convection with a characteristic velocity $V_c=(q_0 a g/\rho_0 h_0)^{1/3}=a/t_c$ (see Refs. 1 and 2). Here ρ_0 is the density and h_0 is the enthalpy of unperturbed medium, a is the typical transverse size of a beam, g is the acceleration due to gravity, $q_0=\alpha I_0$ is the typical power per the unit volume, α is the absorption coefficient and I_0 is the typical radiation intensity.

At the relatively small fluctuations in hydrodynamical parameters, the gravitational convection is described by the nonlinear system of Boussinesq's equations on the basis of which the classification of regimes of thermal blooming in gases and liquids was proposed.[3,4] In gas media and in some widespread liquids (for example, in water) where the Prandle number $\mathrm{Pr} = \mu_0 C_{p0}/k_0$ (here μ_0 is the coefficient of dynamic viscosity, k_0 is the coefficient of thermal conductivity, and C_{p0} is a specific heat of medium) is the quantity of an order of unity, there the effects of thermal conductivity and viscosity manifest themselves under the same conditions.

Let us relate the density ρ to ρ_0, pressure p to the initial value p_0, temperature T to the corresponding value in unperturbed medium T_0, heat to C_{p_0}, thermal conductivity coefficient to k_0, dynamic viscosity coefficient to μ_0, transverse coordinates x, y to the beam radius a, the time t to t_c, and velocity components U, V – to V_c. Let us direct the z axis along the beam path while the y axis –– opposite to the vector of gravitational field intensity $\mathbf{g} = -\mathbf{e}_y g$ (where $\mathbf{e}_y$ is the unit vector along the y axis). By expanding the hydrodynamic parameters into the series over the small parameter $\varepsilon = q_0 a/(\rho_0 h_0 V_c) = q_0/(\rho_0 h_0)^{2/3}(a/g)^{1/3}$, we will obtain the following system of dimensionless equations for the main terms of fluctuated quantities:

$$\rho = 1 + \varepsilon \rho_1 + \ldots ; \; T = 1 + \varepsilon T_1 + \ldots ;$$

$$p = 1 + \mathrm{Eu}\,(- y/\mathrm{Fr} + (\varepsilon/\mathrm{Fr})\, p_1 + \ldots) ; \; \mathrm{Eu}/\mathrm{Fr} \ll 1 ;$$

$$\mathrm{div}\, \mathbf{V} = 0 ; \qquad (1.1)$$

$$\frac{d\mathbf{V}}{dt} = - \nabla p_1 + \mathbf{e}_y \rho_1 + \frac{1}{\mathrm{Re}} \Delta \mathbf{V} ; \; \frac{d}{dt} = \frac{\partial}{\partial t} + (\mathbf{V}, \nabla) ; \qquad (1.2)$$

$$\frac{d\rho_1}{dt} = - I(x, y, z, t) + \frac{1}{\mathrm{Pe}} \Delta \rho_1 ; \qquad (1.3)$$

$$T_1 = - \rho_1 . \qquad (1.4)$$

Here $\mathrm{Eu} = \rho_0 V_c^2/p_0$ is the Euler number, $\mathrm{Fr} = V_c^2/ag$ is the Froude number, $\mathrm{Re} = \rho_0 a V_c/\mu_0$ is the Reynolds number, and $\mathrm{Pe} = \rho_0 a V_c/k_0 C_{p0} = \mathrm{Pr}\,\mathrm{Re}$ is the Peclet number. In approximation of paraxial beams, for which $a/L \ll 1$ (L is the typical path length), the coordinate z enters system (1) as the parameter, since the changes in the hydrodynamic quantities along the z axis on a scale of transverse size a can be neglected. In the case Pe, Re < 1 the thermal conductivity and viscosity predominate, while gravitational convection cannot virtually be observed. At Pe, Re $\gg$ 1 the viscosity and thermal conductivity of a gas can be neglected. Such a case of strong gravitational convection was discussed in Ref. 5. At Pe, Re ~ 1 there occurs a heat–conducting mode of gravitational convection or heat–conducting convective mode. In this paper, the solution, including two above cases (Pe, Re > 1) is obtained. Owing to absence of perturbations at the initial instant of time, the following conditions must hold:

$$\rho_1|_{t=0} = 0 ; \quad p_1|_{t=0} = 0 ; \quad \mathbf{V}_1|_{t=0} = 0 ; \quad T_1|_{t=0} = 0 ; \qquad (2)$$

We introduce the vorticity function $\boldsymbol{\Omega} = \mathrm{rot}\, \mathbf{V}$ and function of flow ψ: $U = \partial\psi/\partial y$ and $V = - \partial\psi/\partial y$. The system of equations (1) can be written in the following standard form, convenient for integration[6,7]:

$$\frac{\partial A}{\partial t} + \frac{\partial B}{\partial x} + \frac{\partial C}{\partial y} = H ; \qquad (3)$$

$$\omega = - \Delta\psi \qquad (4)$$

$$A = \begin{pmatrix} \omega \\ \rho_1 \end{pmatrix} ; \quad B = \begin{pmatrix} \omega \dfrac{\partial\psi}{\partial y} & - \dfrac{1}{\mathrm{Re}} \dfrac{\partial\psi}{\partial x} \\ \rho_1 \dfrac{\partial\psi}{\partial y} & - \dfrac{1}{\mathrm{Pe}} \dfrac{\partial\rho_1}{\partial x} \end{pmatrix} ;$$

$$C = \begin{pmatrix} - \omega \dfrac{\partial\psi}{\partial x} & - \dfrac{1}{\mathrm{Re}} \dfrac{\partial\omega}{\partial y} \\ - \rho_1 \dfrac{\partial\psi}{\partial x} & - \dfrac{1}{\mathrm{Pe}} \dfrac{\partial\rho_1}{\partial y} \end{pmatrix} ; \qquad H = \begin{pmatrix} - \dfrac{\partial\rho_1}{\partial x} \\ - I \end{pmatrix} . \qquad (5)$$

At the boundary of calculational zone, in the case of the solid surface, the conditions of nonflowing and adhesion must be satisfied

$$\left.\frac{\partial\psi}{\partial x}\right|_{y=\pm L_y/2} = \left.\frac{\partial\psi}{\partial y}\right|_{x=\pm L_x/2} = 0 ; \qquad (6)$$

0235-6880/93/12 864-05 $02.00

$$\left.\frac{\partial\psi}{\partial x}\right|_{x=\pm L_x/2} = \left.\frac{\partial\psi}{\partial y}\right|_{y=\pm L_y/2} = 0 . \quad (7)$$

In open space, assuming that dimensions of calculational zone L_x, L_y are great enough in comparison with a, it will be necessary for "soft" boundary–value conditions defined for the function of flow ψ to be satisfied

$$\left.\frac{\partial\psi}{\partial y}\right|_{y=\pm L_y/2} = \left.\frac{\partial\psi}{\partial x}\right|_{x=\pm L_x/2} = 0 . \quad (8)$$

At the initial instant of time, the following conditions must hold

$$\rho_1|_{t=0} = 0 ; \ \omega|_{t=0} = 0 ; \ \psi|_{t=0} = 0 . \quad (9)$$

In approximation of paraxial optics the beam propagation is described by a dimensionless equation for the complex function of electromagnetic field u with the boundary–value conditions:

$$-2\,i\,F\frac{\partial u}{\partial z} + \Delta_\perp u + (2\,F^2 N\,\rho_1 - i\,N_\alpha F)\,u = 0 ; \quad (10)$$

$$u|_{z=0} = u_0(x, y); \ u|_{x,y\to\pm\infty} = 0 . \quad (11)$$

The field function u is related to the radiation intensity via the equation $I = uu^*$; the Fresnel number is equal to $F = 2\pi a^2/(\lambda L)$, where λ is the radiation wavelength; the absorption parameter $N_\alpha = \alpha L$; the parameter of thermal blooming $N = (L/z_T)^2$, where $z_T = \alpha/\sqrt{\varepsilon(n_0 - 1)/n_0}$ is the typical length of thermal blooming. The initial function u_0 for the collimated Gaussian beam is equal to $u_0(x, y) = \exp[-(x^2 + y^2)/2]$ while for the circular beam – to $u_0(x, y) = \sqrt{[\exp(-r^2) - \exp(-A^2 r^2)]/(1 - 1/A^2)}$; $r = \sqrt{x^2 + y^2}$, where $A = a/a_1$, a_1 is the internal radius of a circle.

One of the first algorithms for numerical simulation of the system of Eqs. (3)–(5) and (10) was proposed in Ref. 7. Numerical solution of this problem, in thin–lens approximation[8] was compared with performed earlier fundamental experimental investigation of thermal blooming under conditions of gravitational convection.[9] In Ref. 10 the nonstationary solution of equations of gravitational convection as applied to the beam in a cell was obtained. Stationary (steady) thermal blooming under conditions of gravitational convection was discussed in Ref. 11. Hydrodynamics equations were solved by the setting method while the paraxial equations – by the three–layered conservative finite–difference scheme of the second order of approximation. The unsteady regime of thermal blooming has been numerically investigated in Ref. 12. The Boussinesq's equations were solved by the explicit two–steps finite–difference Lax–Wendroff scheme. In this paper equations (10) were solved based on the expansion in the discrete Fourier series using the Fourier fast transform.[13] The finite–difference scheme[14] of the second order of approximation was applied to equations (3) and (5)

$$\tilde{A}_{ij} = A^n_{ij} - \frac{\Delta t}{\Delta x}(B^n_{i+1,j} - B^n_{i,j}) - \frac{\Delta t}{\Delta y}(C^n_{i,j+1} - C^n_{i,j}) + \Delta t\,H^n_{i,j}; \quad (12)$$

$$A^{n+1}_{ij} = \frac{1}{2}\left(A^n_{ij} + \tilde{A}_{ij} - \frac{\Delta t}{\Delta x}(\tilde{B}_{ij} - \tilde{B}_{i-1,j}) - \right.$$

$$\left. - \frac{\Delta t}{\Delta y}(\tilde{C}_{ij} - \tilde{C}_{i,j-1}) + \Delta t\,\tilde{H}_{ij}\right) . \quad (13)$$

Peculiar feature of the problem of thermal blooming is in the fact that it is necessary to know exactly the fields of density fluctuations within the radiation–occupied region while the region of fluctuation in hydrodynamic quantities exceeds considerably the dimensions of heat–release zone. A simple approach to setting of "soft" boundary–value conditions of type (8) at the extremely close distance from the beam allows one to reduce considerably the calculational time expended in the tasks of thermal blooming for open space, or, for cell walls far removed from the beam. The analysis shows that in the wide range of similarity parameters N, F, Pe and others the boundary–value conditions can be changed and prescribed at the distance of three–four transverse dimensions of the heat–release zone within error of less than 1%. Analogous approach to the change of boundary–value conditions for the pressure fluctuations (velocity and gas density) was used in Ref. 15 to construct the solution of the problem of thermal blooming of pulsed radiation in the homogeneous gas flow of high rate.

Let us go on to discuss the results. We consider a circular beam with $A = 3$. Figure 1 shows the isochores (at the left, $\rho_1 = 0.1,\ 0.5,\ 0.9\,\rho_{1\min}$) and lines of identical values of the vertical component of rate (at the right $V = 0.9,\ 0.5,\ 0.1\,V_{\min},\ 0.01,\ 0.5$, and $0.9\,V_{\max}$) for the closed volume (Fig. 1*a*) and for open space (Fig. 1*b*) at the instants of time, when the fields of hydrodynamic quantities are close to stationary or quasistationary ones. The dimensions of calculational zone in terms of physical variables are L_x, $L_y = 6.4\,a$. For the case of open space, it is found that the further increase of dimensions (for example, by a factor of two) does not result in noticeable change in perturbation of hydrodynamical parameters. The Peclet and Reynolds numbers are large: Pe = 42 and Re = 56.

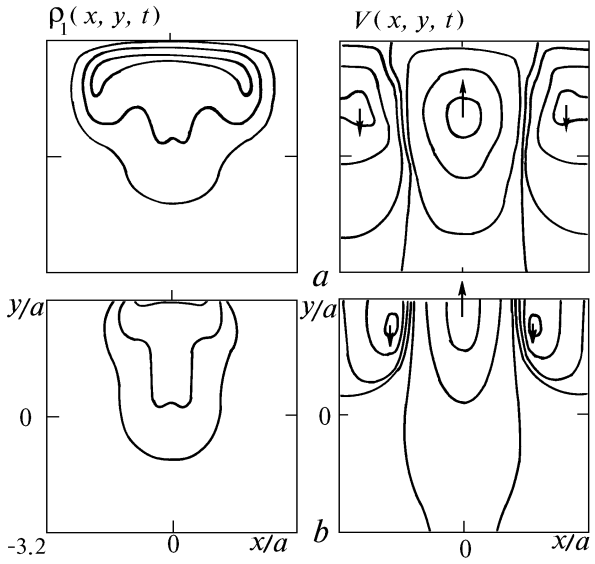

*FIG. 1. Isochores (at the left) and isotaches (at the right) for the vertical component of the rate of gravitational convection caused by the horizontally propagating circular beam ($A = 3$): in the close volume $L_x = 6.4a = L_y$, $t = 5t_c$ (*a*) and in open space, $t = 4t_c$, Pe = 42, and Re = 56 (*b*).*

The selected initial distribution of intensity is characterized by large gradients over transverse coordinates. Therefore, density perturbations can strongly differ one from another even at the large but different Peclet and Reynolds numbers. Figure 2 shows the density perturbations at the center of a beam $\rho_1(0, 0, t)$ as a function of time. Perturbations reach the maximum first in open space (curve *1*) at $t = 2.2\,t_c$, then in a wider tube (curve *2*) at $t = 2.4\,t_c$, and finally in a narrow tube (curve *3*) at $t = 2.8\,t_c$. The increase in the Peclet and Reynolds numbers by about an order of magnitude (compare curves *2* and *4*) leads to a slight increase in maximum itself of perturbation of the function ρ_1 and in its time of achieving $t = 2.6\,t_c$. However before this instant of time, as comparison of curves *2* and *4* shows, the neglected viscosity and thermal conductivity for variant *2* result in the 100% error in determining the density perturbations. The error of the same order occurs also for density perturbation gradients by which the local angles of beam deviation and hence intensity redistribution along the beam path can be found. The values of the function ρ_1 differ one from another by 10% at Pe = 113 and 244, i.e., the error in neglecting of viscosity and thermal conductivity can be considerably less.

Table I shows the temporal and spatial dependences of intensity peaks $I_m = \max\limits_{x,y} [I(x, y, z, t)]$, mean radius $r_m = \int\int (x^2 + (y - \Delta y)^2) I \mathrm{d}x\mathrm{d}y / W$, and displacements of the center of gravity of intensity distribution $\Delta y = \int\int y I \mathrm{d}x\mathrm{d}y / W$, where $W = \int\int I \mathrm{d}x\mathrm{d}y$ is the total power of a beam with account of and without account of viscosity and thermal conductivity at the following values of similarity parameters: $F = 10$; $N = 1$; $N_\alpha = 0.1$, Pe = 10, Re = 13.2. The initial distribution of intensity over a beam is circular, $A = 3$. A comparison of results shows that the neglect of thermal conductivity results in an error in calculations of local parameters up to 138% ($t/t_c = 2$; $z/z_T = 0.4$). An error in calculation of relative displacement $\Delta y/a$ reaches 84% ($t/t_c = 2$, $z/z_T = 0.6$). Neglected thermal conductivity and viscosity affect slightly the quantity of the mean beam radius, the error achieves only 5.6% ($t/t_c = 7$; $z/z_T = 1$).

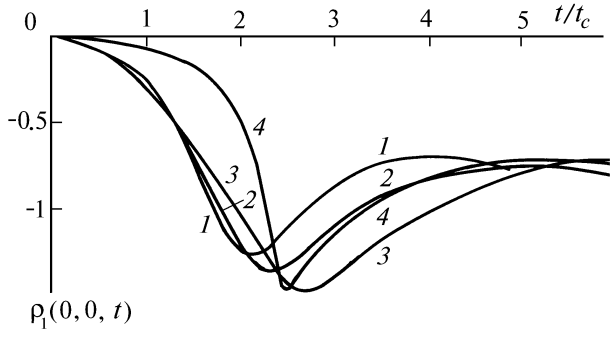

FIG. 2. Temporal dependence of density perturbation at the center of circular beam ($A = 3$): *in open space,* Pe = 42, Re = 56 *(1), in the horizontal tube,* $L_x = 6.4a = L_y$, Pe = 42, Re = 56 *(2), in more narrow tube,* $L_x = 6.4a = L_y$, Pe = 42, Re = 56 *(3), in less thermal conducting and viscous gas,* $L_x = 6.4a = L_y$, Pe = 244, Re = 343 *(4).*

TABLE I. Effect of the account of thermal conductivity (Pe = 10) *and viscosity* (Re = 13.2) *for the circular beam* ($A = 3$) *on the intensity peak* I_m/I_0, *mean radius of a beam* r_c/a, *and displacement of the center of gravity* $\Delta y/a$.

t/t_c	$(z/z_T = 1)$	1	2	3	5	7
I_m/I_0	Pe = ∞	0.588	0.615	1.08	0.589	0.610
	Pe = 10	0.714	0.573	0.605	0.630	0.603
r_c/a	∞	1.26	1.42	1.33	1.265	1.32
	10	1.24	1.36	1.32	1.22	1.25
$\Delta y/a$	∞	− 0.0095	− 0.119	− 0.273	− 0.107	− 0.149
	10	− 0.0065	− 0.071	− 0.203	− 0.140	− 0.119
z/z_T	$(t/t_c = 2)$	0.2	0.4	0.6	0.8	1
I_m/I_0	∞	0.843	1.50	1.33	1.04	0.615
	10	0.722	0.631	0.733	0.691	0.573
r_c/a	∞	1.07	1.11	1.19	1.29	1.42
	10	1.07	1.11	1.17	1.25	1.36
$\Delta y/a$	∞	− 0.006	− 0.217	− 0.0461	− 0.0792	− 0.119
	10	− 0.0036	− 0.0135	− 0.0285	− 0.0478	− 0.071

Thus, even at large values of the Peclet and Reynolds numbers, being equal to $\sim 10^1$, the neglected viscosity and thermal conductivity can result in the considerable error in determining the fluctuating parameters of the beam, in particular, maximum intensity along the path.

The error in neglect of viscosity and thermal conductivity at Pe, Re $> 10^1$ is considerably less for relatively smooth dome–shaped distributions, for example, Gaussian distribution. In the laboratory experimental investigations of propagation and thermal blooming of laser beams, at small transverse dimensions of a beam $\sim 10^{-3}$ and moderately low powers ~10 W, the Peclet and Reynolds numbers are of an order of unity. In addition, it is also necessary to account for dissipative processes in a gas.

Let us consider thermal blooming of Gaussian beam, under conditions identical to the experimental ones.[9] The experiments were carried out in the gas cell in the form of metallic tube with the end windows made of NaCl, being transparent for CO_2–laser radiation ($\lambda = 10.6$ μm). The tube length is $L = 1.5$ m, beam radius is $a = 0.003$ m, and tube radius is $R = 2.85 \cdot 10^{-2}$ m. Since the cross section size of the tube is larger than that of the beam by an order of magnitude, the calculations were carried out according to the algorithm for open space. Absorption coefficient α was varied by addition of small amounts of propane–butane gas mixture to nitrogen (working gas in the cell), the density ρ_0 and refractive index n_0 were varied by the change in pressure from 1 to 10 atm. The power of a beam was equal to 7–9 W. Thus, the experiment conditions made it possible to vary independently the absorption parameter N_α and thermal blooming parameter N. The Fresnel number was equal to 3.56.

The experimental and calculational isophotes are shown in Fig. 3. The lines are plotted for similar intensities $I = 0.2$; e^{-1}; $0.5 I_m$ within the limit of stationary state of thermal blooming. In Fig. 3*a* isophotes correspond to the absorption coefficient $\alpha = 0.13$ m^{-1}, power $W_0 = 1.2$ W, and pressure $p_0 = 1$ atm. The characteristic time of convection is $t_c = 0.270$ s, $V_c = 0.0111$ m/s, $N_\alpha = 0.195$, $N = 0.316$, Pe = 1.61, Re = 2.15, and the scale of density perturbation is $\varepsilon = 0.0421$. Under standard conditions unchanged refractive index is taken to be equal to $n_0 = 1 + 3 \cdot 10^{-4}$ in nitrogen. For isophotes in Fig. 3*b* $\alpha = 0.22$ m^{-1}, $W_0 = 2.2$ W, and

p = 2 atm. The following values: t_c = 0.24 s, V_c = 0.0125 m/s, N_α = 0.330, N = 0.794, Pe = 3.61, Re = 4.83, and ε = 0.0529 correspond to the above conditions. Isophotes in Fig. 3*c* are plotted for the values: $\alpha = 0.66$ m^{-1}, W_0 = 4.4 W, p_0 = 5 atm, t_c = 0.174 s, V_c = 0.0172 m/s, N_α = 0.99, N = 3.79, Pe = 12.5, Re = 16.7, and ε = 0.101. Prandtl number for nitrogen is equal to 0.72.

The last variant of isophotes (Fig. 3*c*) should be assigned to mode of developed (or pure) gravitational convection (Pe, Re $\gg$ 1), variant 3*b* – to thermal conducting convective mode, and variant 3*a* is close to merely thermal conductive mode in which heat release is negligibly small due to convection. Let us note that as follows from the structure of analytical solutions of thermal conductivity equation, the relationship between the convective and thermal conductive modes of heat release is characterized by the parameter Pe/4, for variant 3*a* it is less than unity. The contours plotted for similar intensity from numerical calculations agree quite well with experimental ones, at least for variants 3*b* and 3*c*. There are some quantitative differences in the value of displacement of intensity peak and of more upward prolonged "wings" of half moon (in experimental result).

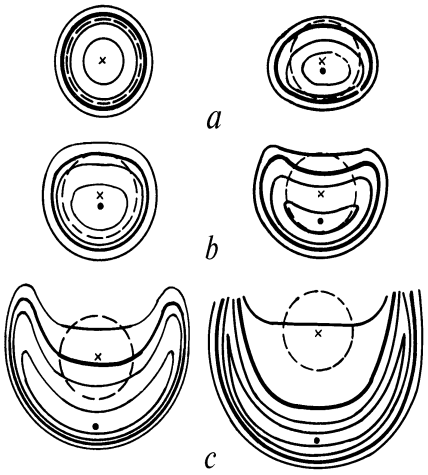

FIG. 3. A comparison of theoretical (at the left) and experimental (at the right) isophotes of steady thermal blooming of Gaussian beam: (a) N = 0.316, N_α = 0.195, Pe = 1.61, $\alpha = 0.13$ m^{-1}, W_0 = 1.2 W; (b) N = 0.794, N_α = 0.330, Pe = 3.61, $\alpha = 0.22$ m^{-1}, W_0 = 2.2 W; and, (c) N = 3.79, N_α = 0.99, Pe = 12.5, $\alpha = 0.66$ m^{-1}, W_0 = 4.4 W,

Nonstationary thermal blooming in the experiment[9] was studied for the case: $\alpha = 0.16$ m^{-1}, W_0 = 9 W, and p_0 = 2 atm. The similarity parameters N_α = 0.24, N = 1.75, Pe = 5.36, Re = 7.17, and following typical gas–dynamical values: t_c = 0.162 s, V_c = 0.0185 m/s, and the scale of density perturbation ε = 0.0117 correspond to the above case.

The temporal dependences of intensity peaks I_m/I_0 (at the top) are shown in Fig. 4*a* and in Fig. 4*b* are depicted the values of its displacement Δy_m caused by thermal blooming: the experimental curves (*1*), theoretical (calculational) (*2*), calculation using variant from Fig. 3*c* (*3*), and calculation using variant from Fig. 3*b* (*4*). Considered theoretical (curve *2*) and experimental (curve *1*) temporal dependences, obtained under the similar conditions agree well qualitatively. The values of intensity peak at the minima are close and equal to $(I_m/I_0)_1 = 0.30$ and $(I_m/I_0)_2 = 0.26$. The instants of time, at which maximum displacement Δy_m of the peak takes place are also close: $(t_{max})_1 = 0.4$ and $(t_{max})_2 = 0.35$ s. But the value of displacement Δy_m is greater by a factor of about 1.5 in the experiment, the same is in Fig. 3*b*. The time for achieving the minimum value of intensity peak is shorter by a factor of more than two in the experiment.

The conditions of performing the experiment are not completely identical to calculation conditions that results in quantitative differences. A comparison of experimental and calculational isophotes in Fig. 3 shows that gravitational convection and thermal blooming are stronger pronounced in the experiment. In calculations the wavefront of a beam at the input to the cell was taken to be plane. In experiments, possibly, there occurred weak additional focusing that resulted in amplification of thermal blooming. Experimental spatial distribution of intensity was measured in series of consequent startings between which the detector with small diagram changed its positions. In so doing at the subsequent startings there were, perhaps, nonzero values of flow rate or temperature gradients (density) of gas in a tube filled with nitrogen that resulted in faster development of convection and partial enhancing of the effect. There is one more possible reason of distinctions, the influence of which one can evaluate.

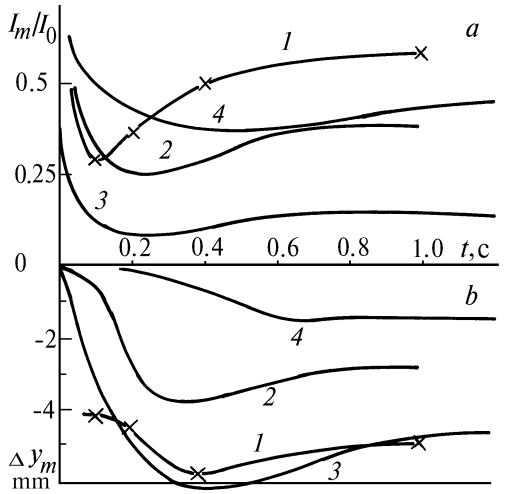

FIG. 4. Temporal dependences of the intensity peak I_m/I_0 (a) and its displacement $\Delta y/\alpha$ (b). Experimental dependence at N = 1.75, N_α = 0.24, Pe = 5.36 (1), theoretical calculation (2), calculation from the variant in Fig. 3c (3), and variant from Fig. 3b (4).

As is shown at the optical arrangement (Fig. 1, Ref. 9), the beam at the cell exit passes a certain distance l (with two rotatable mirrors) before it arrives at the diagram of detector. At the exit of the cell filled with nitrogen not only intensity but the phase of radiation appear to be perturbed, therefore the beam acquires additional divergence angle[16]

$$\theta \sim \frac{a}{L} B_1(L) = \frac{a}{L} N \int_0^1 (\exp(-N_\alpha z)^{2/3}\, dz =$$

$$= \frac{3}{2} \frac{a}{L} \frac{N}{N_\alpha} (1 - \exp(-2N_\alpha/3)) .$$

At the distance l to the diaphragm the additional broadening of a beam for a length of $\Delta r \sim \theta l$ occurs.

Let us consider the results in Fig. 3*c* according to which the theoretically and experimentally determined displacements of intensity peaks differ in $\delta y = 3$mm. Equating this difference to additional broadening Δr we obtain the distance $l = 0.54$ m. Thus, for experiment conditions from variant shown in Fig. 4 at $N = 1.75$ and $N_\alpha = 0.24$ (curve *1*) we obtain that additional displacement Δr and hence the difference δy must be equal to 1.75 mm. Difference in the displacement value Δy_m on curves *1* and *2* (Fig. 4) is close to this value and equal to 2 mm.

Thus, a fair agreement between theoretically and experimentally obtained isophotes is revealed as well as between temporal dependences of intensity peaks and values of its displacements towards the flow of self–induced convection.

REFERENCES

1. S.A. Akhmanov, D.P. Krindach, A.V. Migulin, et al., IEEE J. Quantum. Electron. **QE–4**, No. 10, 568–575 (1968).
2. D.C. Smith, IEEE J. Quantum. Electron. **QE–5**, No. 12, 600–607 (1969).
3. L.R. Bisonette, Appl. Opt. **12**, No. 4, 719–728 (1973).
4. B.P. Gerasimov, V.M. Gordienko, and A.P. Sukhorukov, Zh. Tekh. Fiz. **45**, No. 12, 2485–2493 (1975).
5. A.N. Kucherov, N.K. Makashov, E.V. Ustinov, Izv. Vyssh. Uchebn. Zaved., Radiofizika **35**, No. 2, 145–154 (1992).
6. P.M. Livingstone, Appl. Opt. **10**, No. 2, 426–436 (1971).
7. B.P. Gerasimov, Preprint No. 13, Inst. of Applied Mechanics, Moscow (1975).
8. V.A. Petrishev, L.V. Piskunova, V.I. Talanov, and R.E. Erm, Izv. Vyssh. Uchebn. Zaved., Radiofizika **24**, No. 2, 161–171 (1981).
9. V.A. Petrishev, N.M. Sheronova, and V.E. Yashin, Izv. Vyssh. Uchebn. Zaved., Radiofizika **18**, No. 7, 963–974 (1975).
10. B.P. Gerasimov, V.M. Gordienko, and A.P. Sukhorukov, Inzh.–Fiz. Zh. **36**, No. 2, 331–336 (1979).
11. B.P. Gerasimov, T.G. Elizarova, and A.P. Sukhorukov, Zh. Tekh. Fiz. **53**, No. 9, 1696–1705 (1983).
12. I.A. Chertkova and S.S. Chesnokov, Atm. Opt. **3**, No. 2, 108–114 (1990).
13. J.A. Fleck, J.R. Morris, and M.D. Feit, Appl. Phys. **10**, No. 2, 129–160 (1976).
14. R. Peyre and J. Teylor, *Calculational Methods in Problems of Liquids Mechanics* (Gidrometeoizdat, Leningrad, 1986).
15. V.V. Vorob'ev, M.N. Kogan, A.N. Kucherov, and E.V. Ustinov, Atm. Opt. **2**, No. 2, 164–172 (1989).
16. A.N. Kucherov, N.K. Machev, and E.V. Ustinov, Izv. Vyssh. Uchebn. Zaved., Radiofizika **34**, No. 5, 528–535 (1991), ibid., **36**, No. 2, 135–142 (1993).